



OPEN Unveiling the role of *PPIF* and macrophage subtypes in LSCC progression via single-cell and exosome RNA sequencing

Jianchao Wang^{1,7}, Chunhan Liu^{1,2,7}, Tailin Wu^{3,7}, Lei Tan⁴, Jiangyan Wang⁵, Wenliang Zhang⁶, Yang Liu⁶, Xudong Wei⁵✉ & Di Zhang¹✉

Laryngeal squamous cell carcinoma (LSCC) is a highly aggressive malignancy with a rising incidence over time. The tumor microenvironment (TME) plays a crucial role in LSCC development, yet the precise cellular characteristics of laryngeal cancer and its TME remain unclear. Here, we employed single-cell RNA sequencing analysis to uncover the heterogeneous populations of tumor and immune cells and investigate the role of the TME in LSCC. This analysis revealed significant heterogeneity among malignant cells, T cells, and macrophages. Notably, regulatory T cells were markedly increased at tumor sites, and macrophage analysis identified an increased presence of the Macrophage-C1-C1QC subset with up-regulated *PPIF* expression. Bulk RNA-seq further confirmed *PPIF* up-regulation in exosomes derived from LSCC tissues. Consistently, survival analysis indicated that high *PPIF* expression was associated with poor prognosis in LSCC. Further analyses suggested that *PPIF* up-regulation in Macrophage-C1-C1QC cells was associated with the enhancement of their anti-inflammatory phenotype and the promotion of F11R-F11R signaling with malignant cells, allowing LSCC cells to evade macrophage-mediated cytotoxicity. Our study provides new insights into the cellular dynamics of LSCC and highlights the critical role of Macrophage-C1-C1QC and *PPIF* in LSCC progression, offering potential therapeutic targets for treatment.

Keywords LSCC, Single-cell RNA, Exosomes, Macrophage, *PPIF*

Laryngeal squamous cell carcinoma (LSCC) remains a prevalent neoplasm affecting the head and neck region, constituting approximately 20% of all cases¹. Up to 60% of LSCC patients were diagnosed with an advanced clinical stage (III or IV)². Notwithstanding remarkable progressions in therapeutic modalities encompassing surgery, radiotherapy, chemotherapy, and immunotherapy, the ten-year survival rate for LSCC has demonstrated a decrement over the preceding decades. Consequently, it is imperative to discern innovative, reliable biomarkers for early diagnosis and prognosis that can facilitate therapeutic assessment for individuals afflicted with LSCC.

The tumor microenvironment (TME) is characterized by the interaction of various cell types, including tumor-associated macrophages (TAMs), T cells, tumor cells, and other cells³. The interplay among these distinct cell types within the TME possesses significant correlations with tumor progression and represents a promising therapeutic target³. Numerous studies have demonstrated that the prognosis and malignancy of tumors are largely dictated by the TME⁴. Moreover, the interactions between immune cells and tumor cells play a crucial role in the prognosis of patients with LSCC⁵. Recently, single-cell RNA sequencing (scRNA-seq) is employed to unravel the intricacy of the TME by characterizing the gene expression and immune cell subtypes within tumor

¹Department of Otolaryngology, The Third People's Hospital of Shenzhen (The Second Affiliated Hospital of Southern University of Science and Technology), No.29 Bulan Rd, Shenzhen 518112, Guangdong, China. ²Vertigo Clinic, The Third People's Hospital of Shenzhen (The Second Affiliated Hospital of Southern University of Science and Technology), No.29 Bulan Rd, Shenzhen 518112, Guangdong, China. ³The Key Laboratory of Biomedical Information Engineering of Ministry of Education, School of Life Science and Technology, Xi'an Jiaotong University, Xi'an 710049, Shaanxi, China. ⁴State Key Laboratory of Reproductive Medicine and Offspring Health, Nanjing Medical University, Nanjing 211166, China. ⁵Department of Otolaryngology-Head and Neck Surgery, Gansu Provincial Hospital, No.204 Donggang West Rd, Lanzhou 730000, Gansu, China. ⁶Department of Bioinformatics, Outstanding Biotechnology Co., Ltd.-Shenzhen, No. 5022 Binhe Avenue, Shenzhen 518000, Guangdong, China. ⁷Jianchao Wang, Chunhan Liu and Tailin Wu contributed equally to this work. ✉email: weixd93@lzu.edu.cn; entszsy@163.com

microenvironments⁶. However, while few articles report the scRNA-seq data for LSCC cells, there is a need for more data from different patients to better understand the complex TME of LSCC.

In the context of the expeditious progress of cancer immunotherapy, considerable attention is directed towards the utilization of cell-secreted diminutive vesicles that elicit an immune response. Among these nanoscale vesicles of cellular origin, exosomes hold significant potential in the field of cancer immunotherapy due to their immunogenic properties and ability to transfer molecules⁷. Notably, exosomes originating from tumor cells and immune cells possess distinctive compositional profiles that directly impact anticancer immunotherapy. Furthermore, exosomes are capable of transporting their cargo to specific cells, thereby exerting influence over the phenotype and immune regulatory functions of these targeted cells⁷.

TAMs, as key components of the tumor microenvironment, play a multifaceted role in tumorigenesis and cancer progression. These cells are derived from circulating monocytes that are recruited to the tumor site. Upon recruitment, the local tumor microenvironment influences their polarization into either pro-inflammatory (M1) or anti-inflammatory (M2) phenotypes. M1 macrophages generally exert anti-tumoral effects through the production of inflammatory cytokines, reactive nitrogen and oxygen species, and by presenting antigens to T cells, thereby promoting an immune response against tumor cells. In contrast, M2 macrophages are associated with tumor-promoting activities. They facilitate tumor growth and metastasis by secreting growth factors, promoting angiogenesis, and suppressing adaptive immune responses through the release of anti-inflammatory cytokines. The dynamic balance between M1 and M2 macrophages within the tumor microenvironment is a critical factor in determining the outcome of cancer progression. In laryngeal cancer, the role of TAMs has been highlighted in several studies, suggesting that a high density of TAMs correlates with poor prognosis and enhanced tumor invasiveness.

Peptidylprolyl Isomerase F (*PPIF*) is a protein coding gene. The protein encoded by this gene is a member of the peptidyl-prolyl cis-trans isomerase (PPIase) family. PPIases catalyze the cis-trans isomerization of proline imidic peptide bonds in oligopeptides and accelerate the folding of proteins. This protein is part of the mitochondrial permeability transition pore in the inner mitochondrial membrane. Activation of this pore is thought to be involved in the induction of apoptotic and necrotic cell death. Study identifies an enhancer with an inflammatory bowel disease risk variant that regulates the expression of *PPIF*, influencing the mitochondrial membrane potential in macrophages⁸. Additionally, it demonstrates that *PPIF*, which encodes cyclophilin D, regulates mitochondrial permeability transition and significantly impacts the early inflammatory response in macrophages⁹. However, it remains unclear whether *PPIF* directly regulates macrophages or is associated with the development of LSCC, necessitating further research.

Here, we used single-cell RNA sequencing (scRNA-seq) to analyze tumor and immune cell heterogeneity in LSCC and found significant variation among malignant cells, T cells, and macrophages. Notably, regulatory T cells were increased at tumor sites, and Macrophage-C1-C1QC cells exhibited up-regulated *PPIF* expression. Bulk RNA-seq confirmed *PPIF* upregulation in LSCC-derived exosomes, and high *PPIF* expression correlated with poor prognosis. Our findings highlight the role of *PPIF* in enhancing the anti-inflammatory phenotype of Macrophage-C1-C1QC cells and promoting F11R-F11R signaling, which helps LSCC cells evade macrophage-mediated cytotoxicity, offering potential therapeutic targets for LSCC treatment.

Results

Landscape view of cell composition in tumor tissue in patients with LSCC

To better investigate the TME of LSCC, we collected three tumor tissues and their adjacent normal tissues from patients with diagnosed LSCC (Fig. 1a). The H&E staining of these tissues are shown (Fig. 1b). Then, we used fluorescence-activated cell sorting (FACS) to sort single cells by 7-AAD- for single-cell RNA sequencing. After stringent quality assessment, a total of 40,667 cells (ranging from 5149 to 9704 per sample) were deemed suitable for subsequent analysis in the scRNA-seq dataset. Within these cells, a median of 1,286 genes per cell were detected.

To facilitate a comprehensive exploration of immune cell populations, we performed data normalization and integration by pooling the scRNA-seq data from all samples. Furthermore, the application of the harmony and Seurat v4.2.3¹⁰ R packages enabled dataset de-batching and unsupervised clustering to identify discernible cell populations. After clustering, a total of 22 cell clusters were obtained. Two cell clusters were then manually removed to end up with 20 clusters (Fig. 1c, d and Supplementary Fig. 1a, b). Graph-based clustering¹¹ was used to identify the specific cells from these patients, and 12 main cell types were identified, including T cells, macrophages, mast cells, B cells, fibroblasts, plasma cells, neutrophil cells, pericyte cells, endothelial cells, epithelial cells and malignant cells (Fig. 1e, f). All these cell types were characterized using well-known markers (Fig. 1g and Supplementary Fig. 1c).

The CD4 + T cells, neutrophil cells, and macrophages were increased in the tumor tissues of LSCC compared with their adjacent tissues. Conversely, the proportions of CD8 + T cells and B cells exhibited a decline (Fig. 1e and Supplementary Fig. 1d, e). Consistent with recent investigations¹², we observed considerable heterogeneity in the immune composition across tumors from distinct patients with LSCC. The numbers of different cell type in each patient are presented in Supplementary Table S1.

Heterogeneity of malignant cells of different LSCC patients

A comprehensive assessment of LSCC tumors led to the identification of 4,780 malignant epithelial cells characterized by significant chromosomal copy number variants (CNVs). These variants encompassed large-scale amplifications and deletions of DNA, as compared to the reference data derived from normal epithelial cells (Fig. 2a). The top 100 deregulated genes of these cell types are shown in Supplementary Table S2. It was reported that CNVs can drive the rapid adaptive evolution and progress of human cancer¹³. The data shows that LSCC tumor cells contain several CNVs in the entire chromosome, the amplification variants in chromosomes 1, 12,

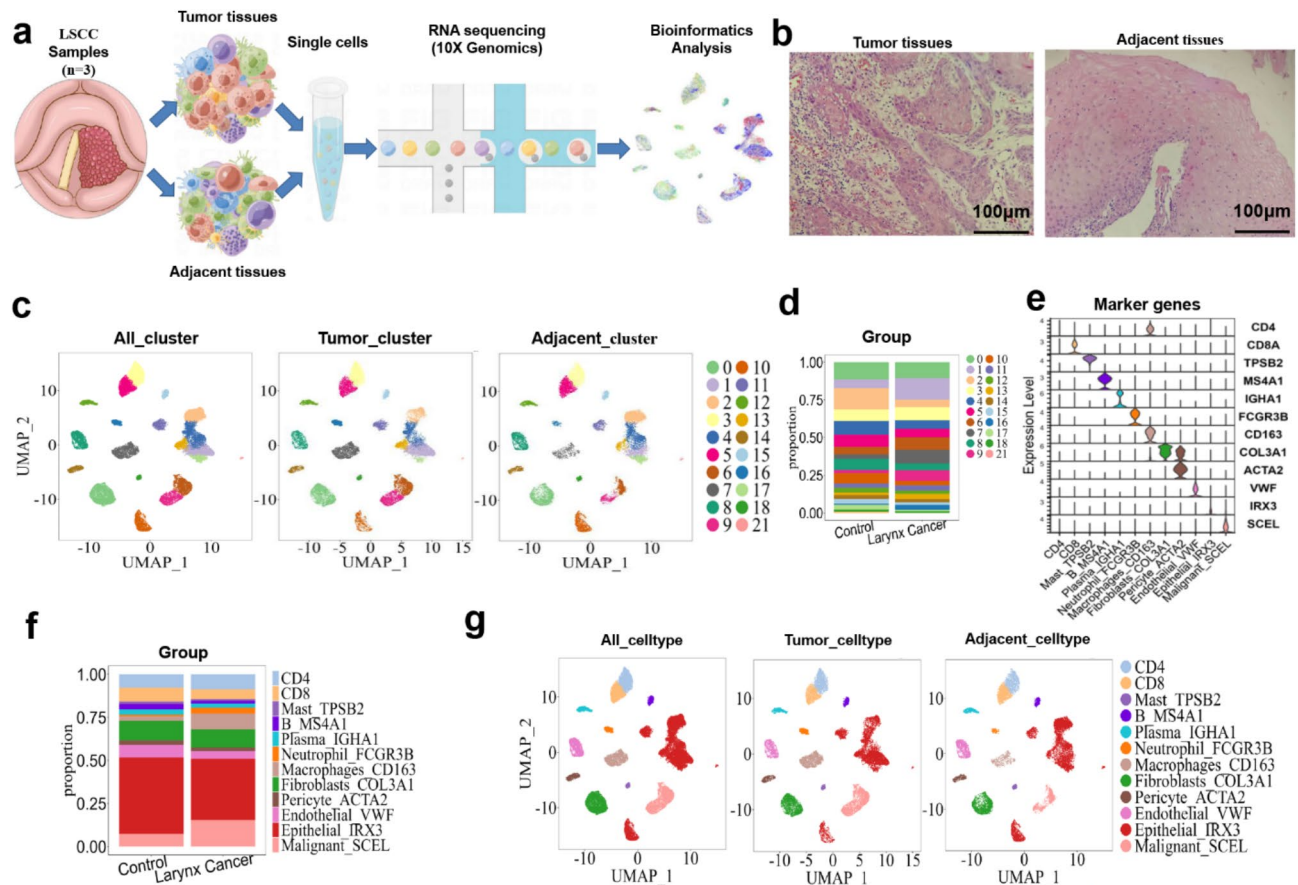


Fig. 1. Landscape view of cell composition in tumor tissue in patients with LSCC. (a) Overview of the study workflow; (b) HE staining of adjacent tissues and LSCC tumor tissues; (c, d) UMAP plot and proportions of each cluster with 40,667 cells from 3 LSCC tumor tissues and 3 LSCC adjacent tissues; (e) The expression of specific marker genes in these cell types; (f) and (g) UMAP plot and proportions annotated by cell types.

20 and the deletion variants in chromosomes 6 and 10 specifically (Fig. 2a). Considering the established role of the *SCEL* gene in the oncogenic progression and tumorigenesis of various human cancers, including LSCC¹⁴, we conducted an investigation into the expression pattern of *SCEL* within the malignant cell population. Based on the presence or absence of detectable *SCEL* transcripts, we categorized these cells into two groups: epithelial cells (*IRX3*) and malignant cells (*SCEL*) (Fig. 2b, Supplementary Fig. 2a). Among the genes co-expressed in tumor tissue and exosomes, the volcano plot highlight genes that are significantly up-regulated or down-regulated (Supplementary Fig. 2b). By comparing the gene expression profiles of tumor tissues and exosomes, researchers can gain insights into the potential roles of exosomes in tumor development and progression.

We further observed that the expression of *ATP5MF*, *NDUFB1* and *UQCRCQ* were up-regulated in tumor malignant cells (Fig. 2c and Supplementary Fig. 2c), which related to the susceptibility of oxidative phosphorylation (OXPHOS)¹⁵. In consistent, we observed specifically higher expression of the major genes involved in OXPHOS and synaptic vesicle pathways as well as chemokine in tumor malignant cells compared to the malignant cells form their adjacent tissues (Fig. 2c, d and Supplementary Fig. 2d). All in all, these results depicted a landscape of the inter- and intra-tumor heterogeneity of the malignant cells in LSCC.

Subtype analysis and altered status of T cells, fibroblasts and neutrophils in LSCC

Since T cells represent the primary cytotoxic immune cells within TME, we proceeded to perform unsupervised clustering of T cells derived from all samples of LSCC. The clustering analysis successfully identified four clusters of *CD4* + T cells, three clusters of *CD8* + T cells, and one cluster of NK/T cells (Fig. 3a). Supplementary Table S3 presents the top dysregulated genes for each cluster. Within the T cell populations, we employed functional markers to discern sub-populations of *CD4* + T cells (including naïve, helper, exhausted, and regulatory T cells) and *CD8* + T cells (including effector and exhausted T cells) (Fig. 3b and Supplementary Fig. 3a). *CD4*-*C1*-*CCR7* exhibited a naïve phenotype, characterized by the expression of *CCR7*, *TCF7*, *LEF1*, and *SELL*, and showed minimal expression of cytokines and effector genes. Treg-*FOXP3* displayed elevated levels of signature genes associated with regulatory T cells, such as *FOXP3*, *IL2RA*, *IKZF2*, and *CTLA-4*, along with co-stimulatory markers like *ICOS*, *TNFRSF9*, and *TNFRSF14*.

Among the *CD8* + T cell clusters, *CD8*-*C1*-*GZMB* and *CD8*-*C2*-*XCL1* exhibited high expression levels of cytotoxic markers such as *GZMB* and *IFNG*¹⁶. Consistent with a recent study¹⁷, the results of our study

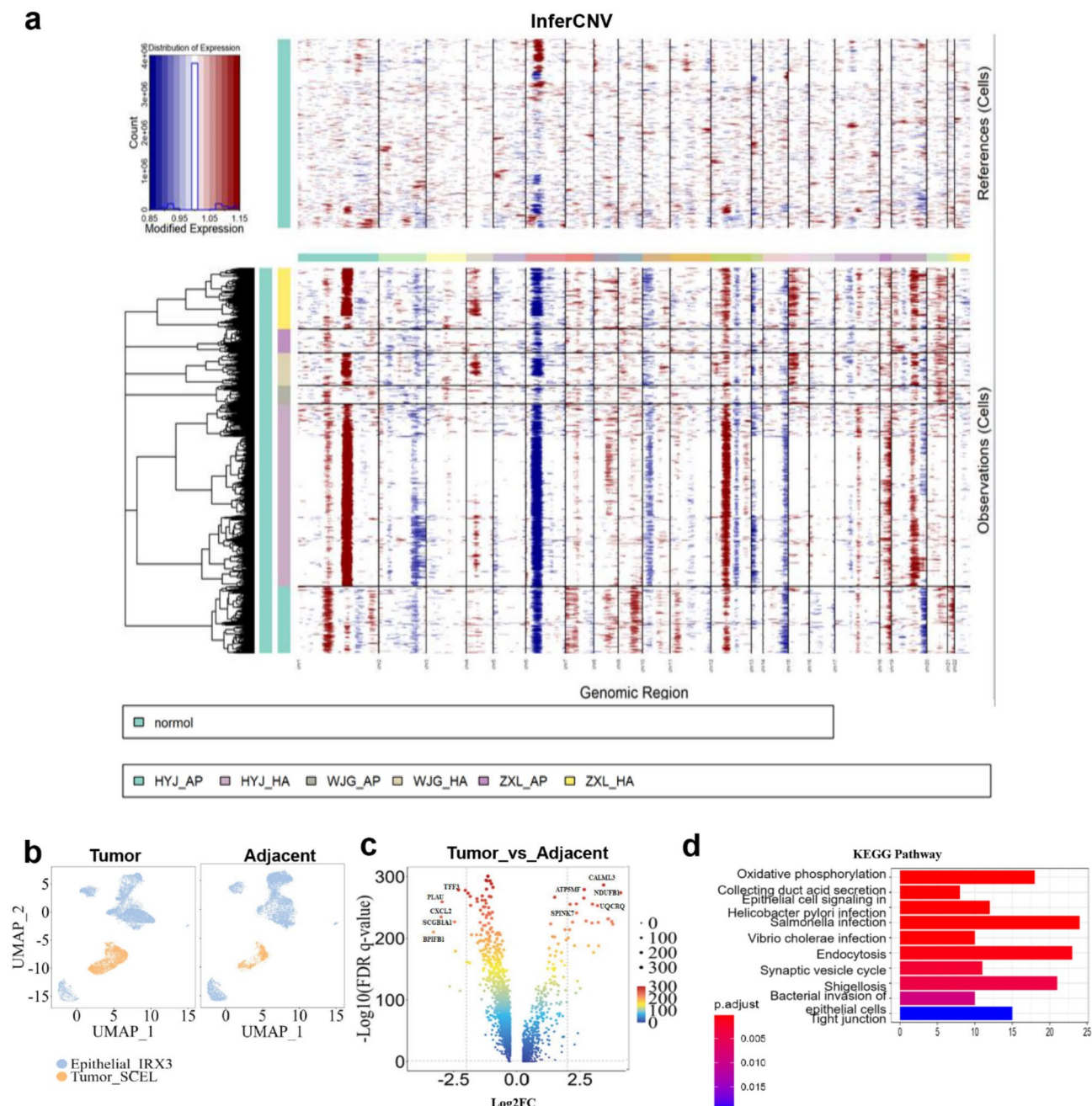


Fig. 2. Heterogeneity of malignant cells with different samples. **(a)** This figure presents an inferCNV analysis of single-cell RNA sequencing data from LSCC patients. The heatmap displays the relative expression of genes across genomic regions, identifying potential copy number variations (CNVs) in different cell populations. The top panel shows the distribution of expression levels in reference cells, which are presumed to have normal CNVs, plotted against various genomic regions. The bottom panel is categorized by patient condition. Color Scale: Modified expression values are indicated on the color scale, with red representing higher expression and blue indicating lower expression relative to the mean. Clusters: Cells are clustered based on the similarity of CNV patterns, with the dendrogram on the left illustrating hierarchical clustering results. Cell Annotations: Cells are annotated with specific identifiers corresponding to different patients and conditions (HYJ_AP, WJG_AP, ZXJ_AP for observations and HYJ_HA, WJG_HA, ZXJ_HA for reference), helping to differentiate between normal and altered genomic expressions; **(b)** UMAP plot of epithelial cells and malignant cells in adjacent and tumor tissues isolated from 3 LSCC patients; **(c)** Volcano plot of tumor tissues compare to adjacent tissues in malignant cells; **(d)** KEGG pathway analysis of deregulated expression gene of LSCC tumor cells.

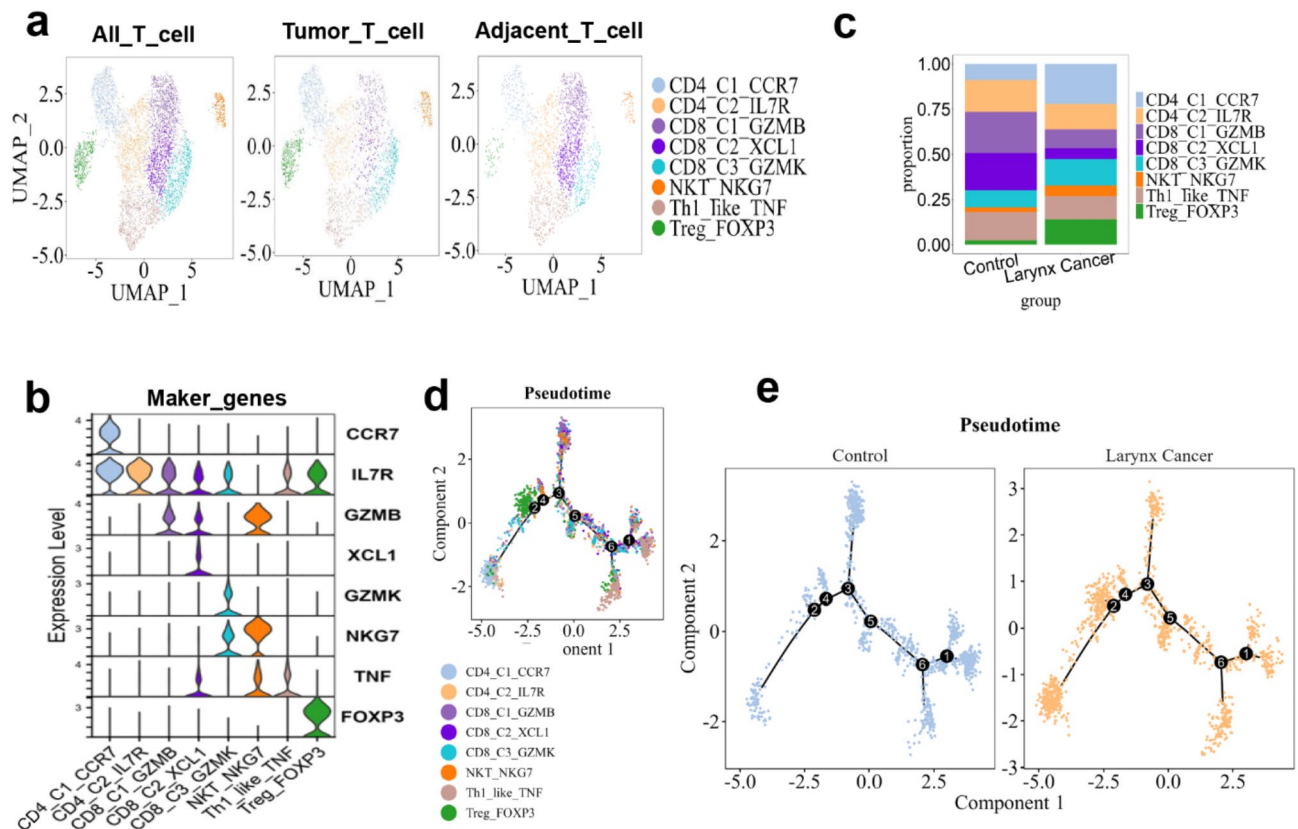


Fig. 3. Subtype analyses and altered status of T cells in LSCC. **(a)** The UMAP plots illustrate the distribution of T cell subsets within all sampled T cells, T cells from tumoral tissues, and adjacent non-tumoral tissues. Each dot represents a single cell, color-coded to indicate different T cell subtypes based on gene expression signatures; **(b)** The expression of specific marker genes in these T cells subsets; **(c)** The bar chart compares the proportion of various T cell subpopulations between control individuals and LSCC patients. The color corresponds to the T cell subsets defined in the UMAP plots, facilitating a direct comparison of cellular composition between health and disease states; **(d)** Diffusion pseudotime analysis in different T cells subsets. **(e)** Diffusion pseudotime analysis of T cells in adjacent and tumor tissues isolated from 3 LSCC patients.

revealed that CD8-C3-GZMK, which acts as a transitional population, exhibited a specific expression profile of transcription factors when compared to the other CD8 clusters. Notably, this population displayed a significantly higher level of *EOMES*. Interestingly, it was observed that this specific cluster was the only one containing cells with elevated levels of *GZMK*, implying a potential association between *EOMES* and *GZMK*. Subsequent investigations confirmed a positive correlation between *GZMK* and *EOMES* in both CD8-C3-GZMK cells and the overall CD8 + T cell population (Fig. 3b, c, and Supplementary Fig. 3a).

Additionally, another cluster (NKT-NKG7) exhibited high expression levels of granzyme genes and *NKG7*, while displaying the lowest expression levels of checkpoint genes, *SELL*, and *TCF7*, indicating a population of recently activated effector T cells (Fig. 3b and Supplementary Fig. 3a). To explore gene networks associated with exhausted CD8 + T cells and regulatory T cells, we utilized publicly available signatures for naive T cells, regulatory T cells, and exhaustion¹⁸.

The distribution of different T cell type in the tumor tissues and their adjacent tissues showed that CD4-C1-CCR7 cells and Treg-FOXP3 cells were increased in the tumor tissues of LSCC. In contrast, the percentages of CD8-C1-GZMB and CD8-C2-XCL1 cells were decreased (Fig. 3c and Supplementary Fig. 3b, c). To trace the origin of intratumoral T cells, we performed pseudotime trajectory analysis and revealed the most terminal status with the highest pseudotime scores for T cells in tumors by using Monocle2 (Fig. 3d, e and Supplementary Fig. 3d). We detected a discernible pattern of pathway enrichment unique to each T cluster, indicative of their diverse functional roles. Particularly, the KEGG pathway analysis¹⁹ demonstrated that the CD4_C1_CCR7 cells in LSCC tumor tissues have different gene expression levels in OXPHOS (Supplementary Fig. 4a). The chemokine signal pathway was highly enriched in CD8_C1_GZMB (Supplementary Fig. 4b), while the antigen processing and presentation was highly enriched in CD8_C2_XCL1 (Supplementary Fig. 4c). In addition, the interleukin-10 production, T cell activation, and NF- κ B signaling pathways were enriched in Treg_FOXP3 (Supplementary Fig. 4d). In short, we identified the distribution and functional pathways of different T cell types in tumor tissues and their adjacent normal tissues of LSCC.

To further evaluate the impact of LSCC tumor cells on fibroblasts, we analyzed the different performance of fibroblasts between the tumor and adjacent tissues of LSCC. The analysis identified a total of 5414 fibroblasts,

which were classified into two clusters by well-known markers in LSCC tissues (Supplementary Fig. 5a). The expression of specific marker genes is presented in Supplementary Fig. 5b. The percentage of subsets of fibroblasts in the tumor and adjacent tissues are shown respectively in Supplementary Fig. 5c. The UMAP plot shown the distribution of these subsets of fibroblasts in the tumor tissues and their adjacent normal tissues (Supplementary Fig. 5a). The data showed that fibroblasts (Fibroblast_COL3A1) and pericyte cells (Pericyte_ACTA2) have no significant change in the LSCC tumor tissues compared with their adjacent tissues (Supplementary Fig. 5c). Then, the KEGG pathway analysis¹⁹ of the clusters of Fibroblast_COL3A1 cells and Pericyte_ACTA2 cells demonstrated the differential gene expression also occurred in the OXPHOS and antigen processing and presentation pathways (Fig. 5d, e), respectively.

To examine the effect of LSCC tumor cells on neutrophils, we analyzed the differential role of neutrophils in the tumor and adjacent tissues of LSCC patients. First, a total of 1334 neutrophils were identified, and they were grouped into two clusters by well-known specific marker genes in LSCC (Supplementary Fig. 6a). The expression of the specific marker genes is shown in Supplementary Fig. 6b. The percentages of neutrophil subsets in tumor and adjacent tissues are shown in Supplementary Fig. 6c, respectively. We used UMAP plots to present the distribution of these neutrophil subsets in the tumor tissue and adjacent tissues (Supplementary Fig. 6a). Our data showed that neutrophils (Neutrophil_FCGR3B) were more abundant in tumor tissues (Supplementary Fig. 6c). In contrast, mast cells (Mast_TPSB2) were reduced in the TME of LSCC tumor tissues (Fig. 5c). GO analysis of Neutrophil_FCGR3B cell clusters indicated that differential gene expression in tumor tissues mainly occurred in positive regulation of cytokine production and immune response regulation signaling pathways (Supplementary Fig. 6d, e).

Distinct functional composition of macrophage cells in LSCC

Subsequently, we performed unsupervised clustering analysis on macrophage cells, which resulted in the identification of five distinct clusters. These clusters encompassed three macrophage clusters, one monocyte cluster, and one dendritic cell (DC) cluster (Fig. 4a–c and Supplementary Fig. 7a, b). Supplementary Table S4 presents the top differentially expressed genes associated with these clusters. Leveraging the validated gene signatures of monocytes, classically activated macrophages (M1), alternatively activated macrophages (M2), and myeloid-derived suppressor cells (MDSCs)¹², macrophage clusters were identified. Macrophage-C3-SNX10, representing the M1; Macrophage-C2-SPP1, representing the M2; Macrophage-C1-C1QC representing MDSC²⁰; Mono-C1-VCAN showed a strong monocyte signature; DC_CD1C was conventional DCs (Fig. 4a–c). The distribution of different macrophage cell type in the tumor and adjacent tissues of LSCC showed that Macrophage-C1-C1QC accounted for the majority of macrophages and increased in tumor tissues (Fig. 4c and Supplementary Fig. 7c). Mono-C1-VCAN and DC_CD1C cells were also increased. In the context of differential expression analysis between the tumor and the adjacent in Macrophage-C1-C1QC cells, heatmap visualize genes that are significantly up-regulated or down-regulated (Fig. 4d).

Through functional enrichment of highly expressed genes, GO analysis can help researchers gain insight into the potential role of Macrophage in the development of aspects such as regulating immune response and apoptosis in LSCC (Fig. 4e). To elucidate the origin of intratumoral macrophages, we employed pseudotime trajectory analysis using Monocle2, which unveiled the Macrophage-C2-SPP1 cells within tumors exhibiting the most advanced state with the highest pseudotime scores (Fig. 4f, g and Supplementary Fig. 7d). Notably, Given that Macrophage-C1-C1QC cells predominate in tumors, limited expression of resident markers may indicate their recent differentiation into Macrophage-C2-SPP1.

PPIF were up-regulated in the Macrophage-C1-C1QC and exosomes derived from the LSCC tumor

To study the differential gene expression in the Macrophage-C1-C1QC cell of LSCC tumor, we performed differential expression analysis and discovered 161 up-regulated genes and 115 down-regulated genes in the Macrophage-C1-C1QC in LSCC tumor tissues compared with those in their adjacent tissues (avg_log2FC > 0.58 and p_val_adj > 0.05) (Supplementary Table S5). In the context of differential expression analysis between the tumor and the adjacent in exosomes discovered 449 up-regulated genes and 98 down-regulated genes (Supplementary Table S6). Through Venn diagram analysis, Macrophage-C1-C1QC and exosomes shared 16 up-regulated genes and 3 down-regulated genes in common (Fig. 5a). The dotplot shows the expression of these co-expressed genes in the single-cell RNA-seq data (Fig. 5b). Volcano plot and heatmap visualize genes that are significantly up-regulated or down-regulated (Fig. 5c, d) and the correlation of these genes in the exosome data (Fig. 5e).

By highlighting genes that are co-expressed between macrophage cells and exosomes, heatmap can help researchers to gain insights into the potential roles of exosomes in regulating immune responses and the development of diseases such as cancer and inflammatory disorders. For example, *PPIF* gene was up-regulated in the Macrophage-C1-C1QC from LSCC tumor tissues (Fig. 5f). This result is consistent with the exosome data we detected. The data showed that the expression of *PPIF* was higher in exosomes derived from tumor than those derived from adjacent tissues (Fig. 5g). We used the GEPIA 2 database to perform prognostic analysis by grouping *PPIF* according to the median value and found that the prognosis of patients with high *PPIF* expression was significantly worse than that of patients with low *PPIF* expression²¹ (Fig. 5h). Furthermore, a published database²² was used to screen drugs and signaling pathways and found 19 drugs and 2 signaling pathways related to *PPIF* anti-apoptotic pathway genes, as shown in Table 1 and Supplementary Table S7.

To elucidate the origin of intratumoral Macrophage-C1-C1QC, we conducted a pseudotime trajectory analysis using Monocle2 (Fig. 4f, g and Supplementary Fig. 7d). Our analysis revealed that Macrophage-C1-C1QC cells were in their most recent state. Given that the pseudotime trajectory analysis mainly positioned macrophages within tumors, and considering their limited expression of resident markers, it suggests that Macrophage-C1-

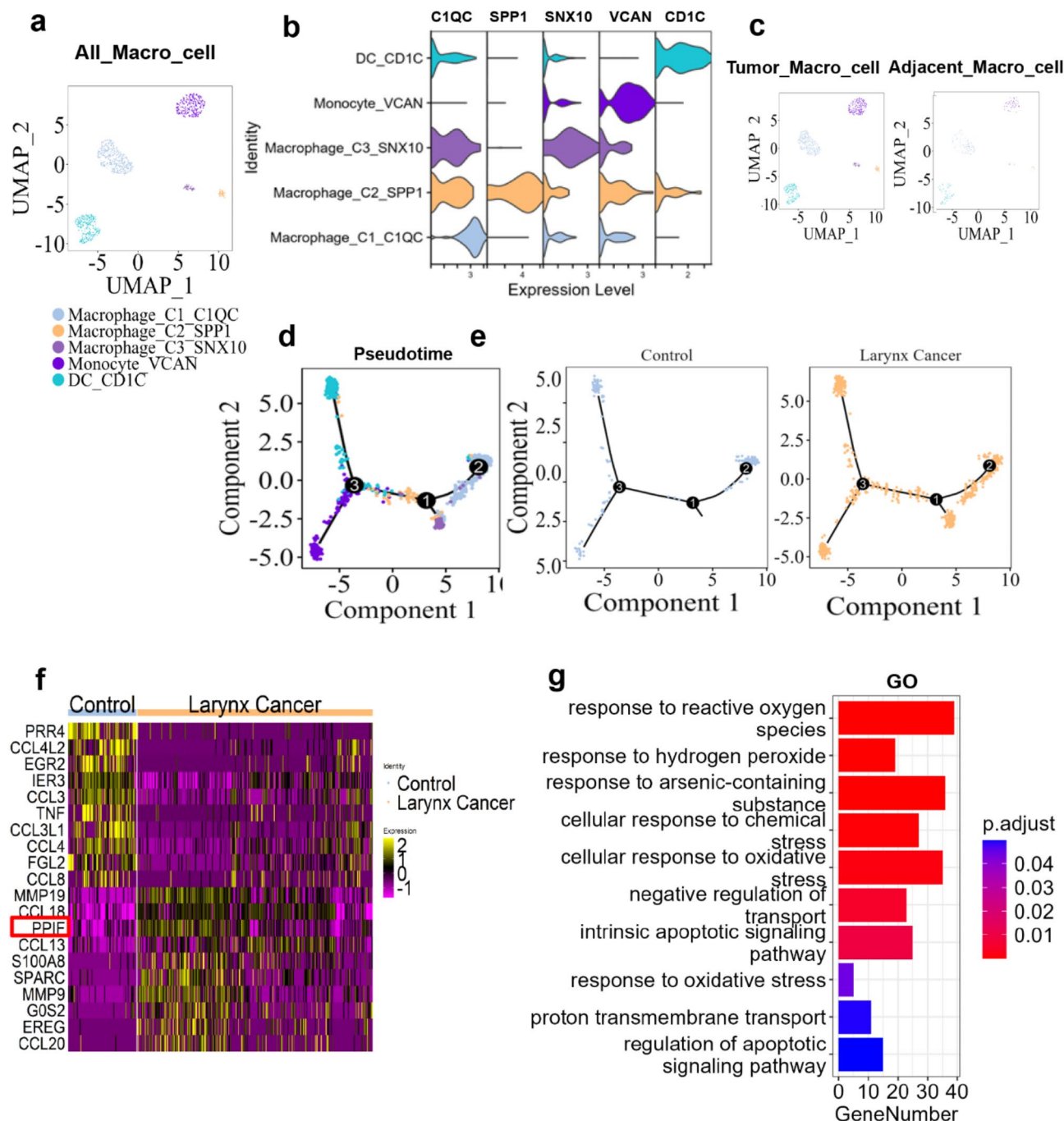


Fig. 4. Distinct functional composition of macrophage cells in LSCC. **(a, c)** UMAP plot of macrophage cells subsets; **(b)** The expression of specific marker genes in macrophage cells subsets; **(d)** Diffusion pseudotime analysis in different macrophage cells subsets; **(e)** Diffusion pseudotime analysis of macrophage cells in adjacent and tumor tissues isolated from 3 LSCC patients; **(f)** Heatmap of different genes of Macrophage-C1-C1QC in adjacent and tumor tissues isolated from 3 LSCC patients; **(g)** GO analysis of deregulated expression genes of Macrophage-C1-C1QC cells.

C1QC cells have a recent influx from the bone marrow. Consequently, the up-regulation of *PPIF* in Macrophage-C1-C1QC may contribute to the immune evasion mechanisms of LSCC tumors. These results indicate that *PPIF* is up-regulated in both macrophages and exosomes within LSCC tumors, underscoring its potential value in the diagnosis and treatment of LSCC.

PPIF is associated with the survival and differentiation of Macrophage-C1-C1QC cell in LSCC

To elucidate the impact of *PPIF* upregulation on Macrophage-C1-C1QC cell function, in total of 277 Macrophage-C1-C1QC cells were extracted from the LSCC tumor tissues. We further used the median of *PPIF*

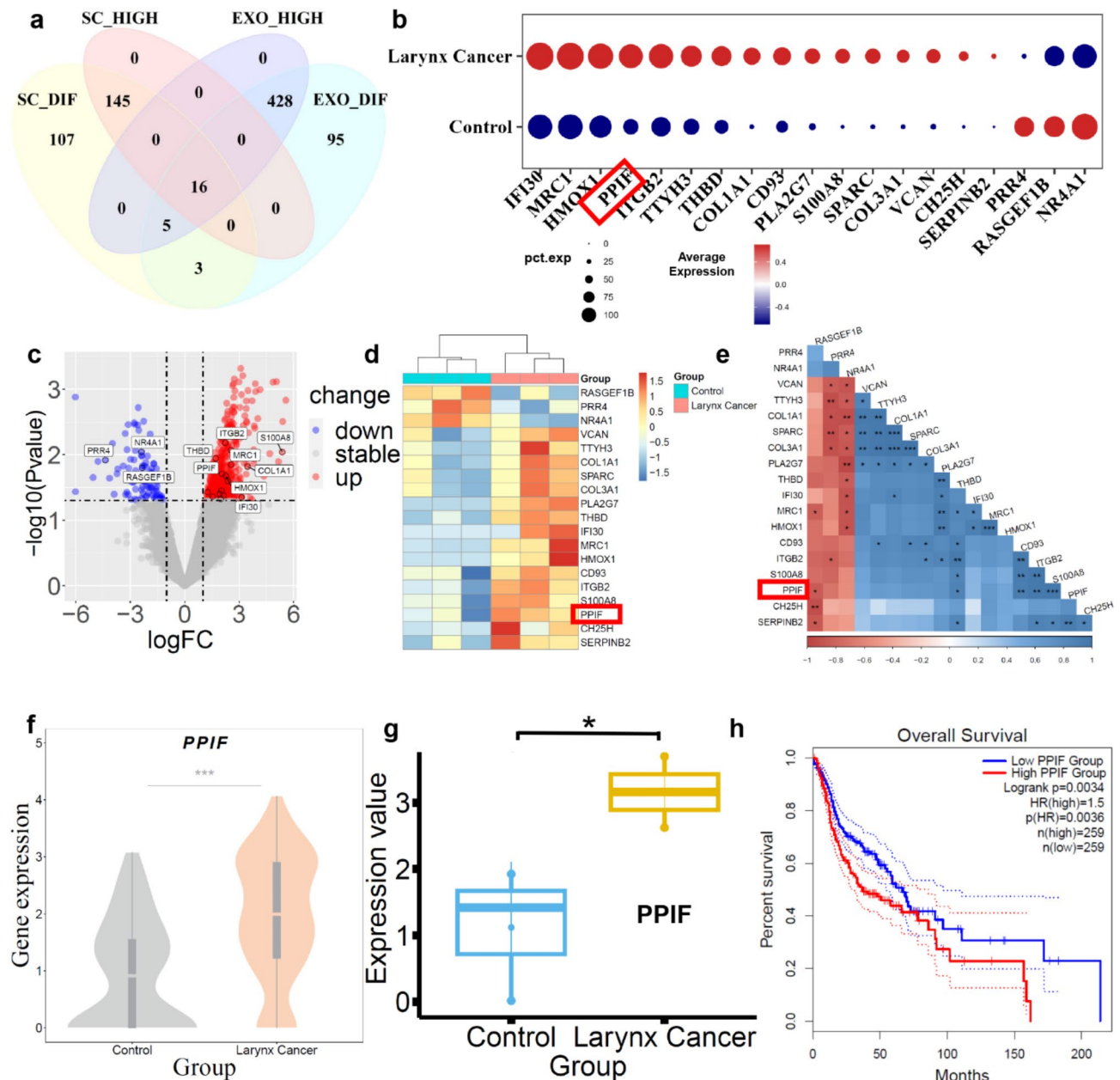


Fig. 5. *PPIF* were up-regulated in LSCC tumor Macrophage-C1-C1QC and exosome. (a) Venn diagram analysis of Macrophage-C1-C1QC differentially expressed genes, highly expressed genes in single-cell transcription data, and differentially expressed genes and highly expressed genes in exosome data; (b) Dotplot of Macrophage-C1-C1QC differentially expressed genes in single-cell transcription data; (c) Volcano of differentially expressed genes in exosome; (d) Heatmap of differentially expressed genes in exosome; (e) Corplot analysis shows the correlation of *PPIF* gene in exosome; (f) Vlnplot of *PPIF* in Macrophage-C1-C1QC of single-cell transcription data; (g) Boxplot of *PPIF* gene in exosome; (h) Survival curve of *PPIF* in Head and Neck Squamous Cell Carcinoma (HNSC) of GEPIA2 database.

gene expression as a standard to divide the Macrophage-C1-C1QC cell population into two subgroups: *PPIF* high expression (Macrophage-C1-C1QC-*PPIF*_high) and *PPIF* low expression (Macrophage-C1-C1QC-*PPIF*_low) groups. Differential expression and functional enrichment analyses revealed that the differential genes between those two subgroups were enriched on the key function pathways associated with the regulation of tumor microenvironment, cell survival and differentiation, such as NF- κ B, phagosome, apoptosis, myeloid cell differentiation signaling pathways (Fig. 6a–e). The top variable genes were showed in Fig. 6c. By performing pseudotime series analysis on the Macrophage-C1-C1QC cell population, we found that there was a certain transformation relationship between Macrophage-C1-C1QC-*PPIF*_high and Macrophage-C1-C1QC-*PPIF*_low subgroups (Fig. 6f–h). These results suggest that the up-regulation of *PPIF* may influence the survival, differentiation, and function of macrophages by affecting the expression of key genes such as *JUN* (Fig. 6c).

No.	Symbol	Drug name	kegg pathway
1	<i>IL1A</i>	Rilonacept	Apoptosis
2	<i>MMP9</i>	Aminoquinuride	Pathways in cancer
3	<i>MMP9</i>	Beclometasone dipropionate	Pathways in cancer
4	<i>MMP9</i>	Budesonide	Pathways in cancer
5	<i>MMP9</i>	Busulfan	Pathways in cancer
6	<i>MMP9</i>	Cefonicid	Pathways in cancer
7	<i>MMP9</i>	Cefotetan	Pathways in cancer
8	<i>MMP9</i>	Cefotiam	Pathways in cancer
9	<i>MMP9</i>	Cefuroxime	Pathways in cancer
10	<i>MMP9</i>	Cefalotin	Pathways in cancer
11	<i>MMP9</i>	Cefradine	Pathways in cancer
12	<i>MMP9</i>	Chlorhexidine	Pathways in cancer
13	<i>MMP9</i>	Dacarbazine	Pathways in cancer
14	<i>MMP9</i>	Econazole	Pathways in cancer
15	<i>MMP9</i>	Floxacin	Pathways in cancer
16	<i>MMP9</i>	Secobarbital	Pathways in cancer
18	<i>MMP9</i>	Zoledronic acid	Pathways in cancer
18	<i>MMP9</i>	Quercetin	Pathways in cancer
19	<i>MMP9</i>	Prazosin	Pathways in cancer

Table 1. The drug-target-pathway interactions with apoptotic signaling pathway.

Consequently, this regulates the tumor immune microenvironment related to the development of LSCC. To further strengthen our findings, we conducted additional analyses, including in-depth single-cell analysis. We observed that, compared to Macrophage-C1-C1QC cells with downregulated *PPIF* expression, those with upregulated *PPIF* expression displayed an increased expression of the immune-suppressive macrophage marker *CD163*, along with the secretion of tumor-promoting cytokines (*IL6*, *VEGFA*, *CCL5*, *MMP1*, *MMP3*, and *MMP9*) (Fig. 6i and j, and Supplementary Fig. 8a). These results further support the notion that *PPIF* up-regulation in LSCC plays a pivotal role in modulating the tumor immune microenvironment and promoting tumor progression.

To further explore inter-patient variability, we performed patient-based subgroup analysis. Notably, one patient did not exhibit detectable Macrophage-C1-C1QC cells, while two other patients did. These two patients, in which Macrophage-C1-C1QC cells were identified, displayed similar expression patterns of *PPIF*, *CD163*, and tumor-promoting cytokines (*IL6*, *VEGFA*, *CCL5*, *MMP1*, *MMP3*, and *MMP9*), with no significant differences between them (see Supplementary Fig. 8b). These results suggest that the heterogeneity of Macrophage-C1-C1QC cells and *PPIF*-related factors across patients may be minimal. However, larger sample sizes and further validation are needed to confirm these findings. Nonetheless, our data indicate that these factors have potential as widely applicable immune therapeutic targets and biomarkers for laryngeal cancer treatment.

Up-regulation of *PPIF* is associated with the anti-inflammatory phenotype of Macrophage-C1-C1QC cells in LSCC

Tumors and their surrounding microenvironments are complex communities of cells that modify local immune cell functions. The interaction between tumor cells and these immune cells are a vital parts of TME. We used a reference list of approximately 1,800 known, literature-supported interactions containing receptor-ligand interactions from the chemokine, cytokine, receptor tyrosine kinase (RTK), and tumor necrosis factor (TNF) families and extracellular matrix (ECM)-integrin interactions²³. Bubble plot showed the ligand-receptor pairs contributing to the signaling between the tumor cells and these immune cell clusters of LSCC (Fig. 7a, b). In LSCC tissues, the interactions of CD209-CECAM1 and APP-CD74 between Macrophage-C1-C1QC cells and malignant cells were significantly reduced compared to adjacent tissues, while these interactions between Macrophage-C1-C1QC cells and Macrophage-C2-SPP1 cells, as well as Macrophage-C3-SNX10 cells, were significantly increased. We found that CD209-CECAM1 and APP-CD74 interactions were present in the LSCC microenvironment compared with adjacent adjacent tissues.

In LSCC tumor tissues, we grouped Macrophage-C1-C1QC cells and divided them into Macrophage-C1-C1QC-*PPIF*_high and Macrophage-C1-C1QC-*PPIF*_low groups based on the median value of *PPIF*. Compared to Macrophage-C1-C1QC-*PPIF*_Low cells, Macrophage-C1-C1QC-*PPIF*_high cells exhibited higher expression of *MRC1* and *CD163*, and displayed a stronger anti-inflammatory phenotype (Fig. 7c). In consistent, further ligand-receptor analysis of the immune microenvironment suggested that Macrophage-C1-C1QC-*PPIF*_high cells specifically exhibited the F11R-F11R ligand-receptor relationship with malignant cells (Fig. 7d, e). This suggests that in LSCC tumors, when Macrophage-C1-C1QC cells were induced to up-regulate *PPIF*, it enhances the F11R-F11R ligand-receptor signaling between macrophages and LSCC malignant cells. Consequently, this allows LSCC malignant cells to evade macrophage-mediated cytotoxicity.

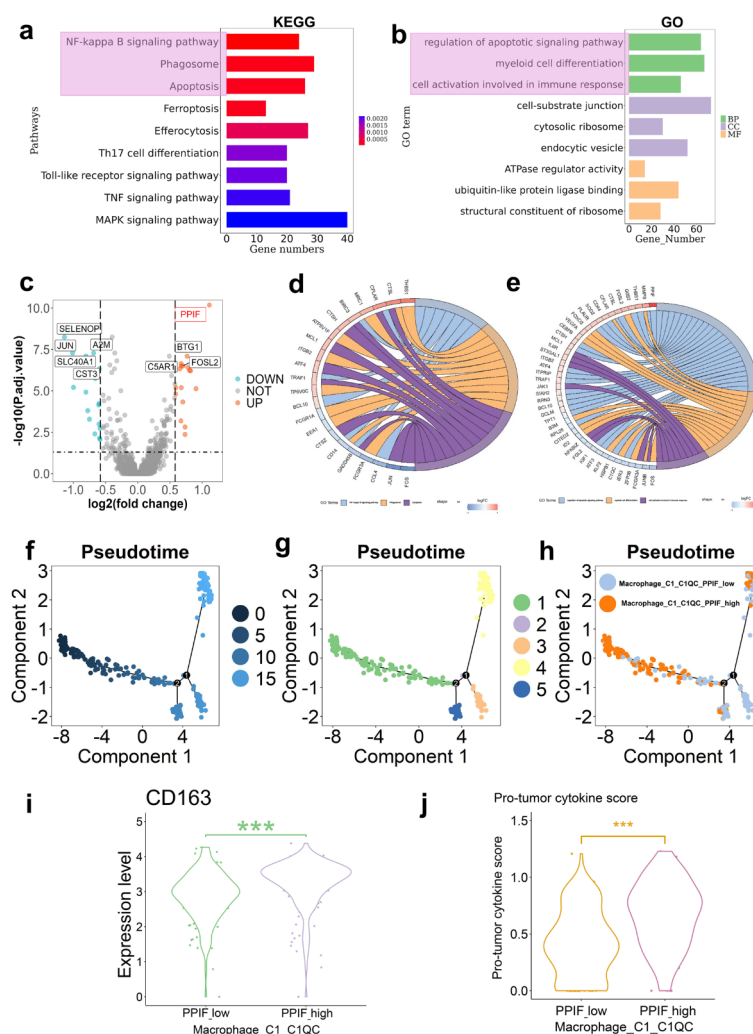


Fig. 6. Function of Macrophage-C1-C1QC_PPIF_high in LSCC tumor. (a, b) KEGG and GO analysis of deregulated expression gene of Macrophage-C1-C1QC_PPIF_high cells; (c) Volcano of differentially expressed genes in Macrophage-C1-C1QC_PPIF_high cells; (d, e) Circular plot displaying genes from three signaling pathways associated with tumor immunity, as identified in KEGG and GO analyses; (f–h) Diffusion pseudotime analysis in Macrophage-C1-C1QC_high cells of LSCC. (i–j) Comparison of CD163 expression and pro-tumor cytokine score between PPIF-high and PPIF-low Macrophage-C1-C1QC cells.

Materials and methods

Experiment model

Human freshly frozen LSCC tissues were collected from The Third People's Hospital of Shenzhen, under their Standard Experimental Ethics Protocol and approved by the Research Ethics Committee of The Third People's Hospital of Shenzhen. After obtaining written informed consent, individuals with suspected or diagnosed LSCC were recruited for participation in this study. Fresh tissue samples were collected during surgical debulking procedures conducted at the primary tumor sites. During surgery, the surgeon sampled the margin of the tumor. The margin may contain invasive front tumor cells. Adjacent non-tumor tissue selected at a certain distance (typically at least 2 cm) from the tumor margin. Although this tissue is near the tumor, it may not contain tumor cells and can serve as a control. The process of tissue acquisition strictly adhered to the prescribed guidelines and regulations.

Cell preparation

Within 48 h of surgery, LSCC tissues underwent enzymatic dissociation to obtain single cells. Cell quantification was performed using the Countstar Rigel S3 instrument with dual-fluorescence AO/PI staining. Following cell sorting, the samples were promptly centrifuged and resuspended in PBS at a concentration of 800–1200 cells/μl, based on the cell count. Subsequently, the Gel Bead-In Emulsions (GEMs) required for the Chromium Controller were generated, and cell barcoding was conducted.

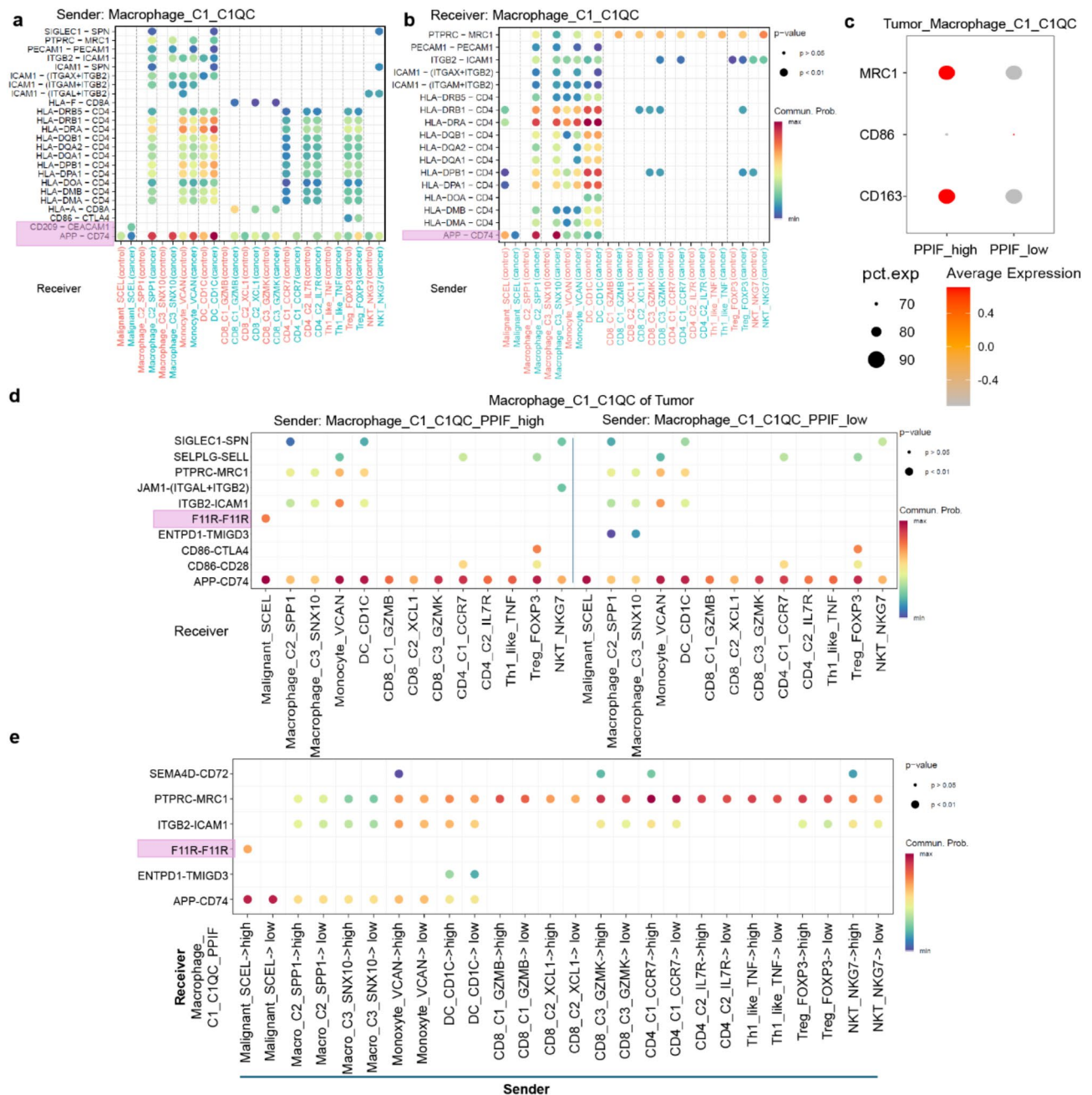


Fig. 7. Bubble plot showed the ligand-receptor pairs contributing to the signaling between the immune cell clusters of LSCC. (a, b) Macrophage-C1-C1QC acts as a ligand and other cell types act as receptors; (c) Dotplot of anti-inflammatory macrophage signature genes; (d) Macrophage-C1-C1QC-PPIF_{high} acts as a ligand and other cell types act as receptors; (e) other cell types act as ligands and Macrophage-C1-C1QC-PPIF_{low} acts as receptors.

Construction of scRNA-seq libraries

For each patient, the construction of 3' Gene Expression Libraries for scRNA-seq was carried out using the Chromium Single Cell Library (v3 chemistry) in accordance with the guidelines provided by the manufacturer (<http://support.10xgenomics.com>).

Analysis of scRNA-seq data

The Seurat v4.2.3 package was employed for the analysis of primary scRNA-seq data. To ensure high-quality data for downstream analysis, we implemented stringent quality control metrics, excluding cells with low-quality or insufficient transcript counts. Specifically, we filtered the data to include genes expressed in at least 10 cells, and cells with gene expression ranging from 500 to 8,000 genes, while mitochondrial transcripts were restricted to less than 20%. To mitigate batch effects and technical variability, the Harmony algorithm²⁴ was applied for

dataset integration, which effectively aligned data from multiple sources and minimized potential confounding effects. This strategy enhanced the robustness and comparability of the integrated dataset. Additionally, we performed rigorous data normalization using the 'SCTransform' within the Seurat pipeline to ensure consistency in gene expression levels across cells, addressing variability due to differences in sequencing depth. Following integration, principal component analysis (PCA) was performed, followed by Uniform Manifold Approximation and Projection (UMAP) for visualization and subpopulation identification. Clear cell clusters were observed, which were subsequently validated through marker gene expression analysis.

For single-cell analysis of cell composition, we used the Seurat package to perform cell type identification and quantify the proportion of different cell populations in tumor and adjacent tissues. The predominant cellular subpopulations within the and immune compartments were delineated based on cluster-averaged gene expression levels of the subsequent gene markers: (1) Malignant: *SCEL*, (2) B cells: *MS4A1*, *CD79A*, (3) CD4 cells: *CD3D*, *CD4*, (4) CD8 cells: *CD3E*, *CD8A*, (5) Macrophage: *CD14*, *CD163*, (6) Fibroblasts: *COL3A1*, (7) Pericyte cells: *ACTA2*, (8) Plasma cells: *IGHA1*, (9) Mast cells: *TPSB2*, (10) Neutrophil cells: *FCGR3B*, (11) Endothelial cells: *VWF*, (12) Epithelial cells: *IRX3*. For in-depth investigation of T cell and macrophage cell populations, the dataset was narrowed down to exclusively include these specific cell types. Subsequently, the data underwent comprehensive processing from its raw form, following the aforementioned methodology.

The examination of T cell and macrophage cell populations in each individual patient was carried out through the division of the subset population based on patients, followed by the processing of raw data according to the previously described methodology.

Pro-tumor cytokine score calculation

The pro-tumor cytokine score was calculated by averaging the expression levels of the tumor-promoting cytokines: "*IL6*", "*VEGFA*", "*CCL5*", "*MMP1*", "*MMP3*", and "*MMP9*". This score was used to quantify the overall expression of these cytokines in macrophage-C1-C1QC cells and to assess their potential role in promoting tumor progression.

InferCNV analysis

The inferCNV tool was utilized to evaluate the initial copy number variations (CNVs) for each region²⁵. CNV was determined by considering the expression level of each cell. Epithelial cells were classified as malignant cells, while other cells were categorized as normal cells.

Monocle analysis

The R package of monocle2 was used to perform the diffusion pseudotime analysis was conducted using the monocle2 software and the results were subsequently transferred back to Seurat.

Cellchat analysis

CellChat²³ is an R package designed for inference, analysis, and visualization of cell-cell communication from single-cell and spatially resolved transcriptomics. CellChat aims to enable users to identify and interpret cell-cell communication within an easily interpretable framework, with the emphasis of clear, attractive, and interpretable visualizations.

Gene expression analysis and functional enrichment analysis

Single-cell gene expression analysis was conducted using Seurat v4.2.3. Differential gene expression between tumor and adjacent tissues was identified using the FindMarkers function, applying the Wilcoxon rank-sum test. Genes with an adjusted p-value < 0.05 and log2 fold change > |1| were considered significant. The differential gene expression analysis of exosome RNA sequencing data was performed using the COVID19db platform (<http://www.biomedical-web.com/covid19db/>)²⁶. This platform enables the processing and comparison of gene expression between different groups, providing insights into the differences in RNA profiles. Functional enrichment analysis was performed using the ClusterProfiler (v3.18.1) package²⁷, with Gene Ontology (GO) and KEGG pathway analyses¹⁹ to explore biological processes and pathways associated with differentially expressed genes. Significant terms (adjusted p-value < 0.05) were visualized using bar and dot plots to highlight key pathways involved in LSCC progression.

Identification of subpopulations

The identified macrophage and T cell clusters were assigned annotations based on the average gene expression profiles of the specified gene markers²⁸: (1) Macrophage: *CD14*, *APOE*, (2) myeloid cells: *SP100A9*, *LYZ*, (3) DC cells: *CD1C*, *CLEC9A*, (4) CD8 T cells: *CD8A*, *CD8B*, (5) CD4 cells: *CD4*, *FOXP3*.

Exosomes isolation

Exosomes were isolated from the serum of subjects with LSCC and vocal cord polyps. To initiate the isolation procedure, the serum underwent filtration by using a 0.45-μm PVDF filter (Millipore, Billerica, MA) in order to remove any cellular debris. The exosomes were harvested by centrifugation of the mixture at 1,5000 g for 30 min under refrigerated conditions (4 °C).

Survival analysis

To evaluate the prognostic value of *PPIF* expression and other key variables, Kaplan-Meier survival analysis was performed using data from TCGA head and neck cancer cohort. Patients were categorized into high and low expression groups based on *PPIF* expression. The log-rank test compared survival distributions between groups, and Cox proportional hazards regression analysis assessed hazard ratios, adjusting for potential confounders.

like age, gender, and clinical stage. A p-value of less than 0.05 was considered statistically significant. Survival analysis was conducted using the survival and survminer packages in R (4.3.1).

Statistic analysis

For pairwise comparisons between groups in the violin plots, we used the Mann-Whitney U test to assess differences in distributions between two independent groups, given that the data did not follow a normal distribution. A p-value of less than 0.05 was considered statistically significant. All statistical analyses were performed using the R programming language (4.3.1) with packages such as ggplot2 for visualization and dplyr for data manipulation.

Discussion

LSCC is an aggressive malignant tumor with limited treatment options and poor patient prognosis. scRNA-seq has shown great potential in understanding the complexity and heterogeneity of LSCC and has led to significant advances in our understanding of the molecular mechanisms underlying LSCC development and progression. The application of scRNA-seq in LSCC has revealed the existence of previously unknown cell subpopulations, which are associated with distinct functional pathways, and have potential clinical significance in the diagnosis and treatment of LSCC. In addition, scRNA-seq has provided new insights into the interactions between LSCC cells and the tumor microenvironment, including immune cells and stromal cells, which are essential for tumor growth and metastasis.

Despite these challenges, the potential benefits of scRNA-seq in LSCC research are clear. By enabling the study of gene expression at the level of individual cells, this technology has the potential to reveal the underlying molecular mechanisms of LSCC, identify new therapeutic targets, and develop personalized treatments that are tailored to the unique genetic profile of individual patients. Immunological therapy is an emerging treatment that may improve the treatment effect and survival time of patients. However, the complex immune microenvironment of LSCC limits the effectiveness and the use of immunotherapy in patients. scRNA-seq is an effective method to understand the immune microenvironment of cancer.

Our study found that OXPHOS-related genes are upregulated in LSCC tumor cells, indicating increased reliance on OXPHOS to support tumor growth, consistent with findings in other cancers^{29–32}. We also observed elevated expression of genes involved in OXPHOS, chemokine signaling, and synaptic vesicle pathways, linking metabolism with immune modulation. KEGG pathway analysis¹⁹ revealed distinct enrichments in T cell clusters: CD4_C1_CCR7 cells showed altered OXPHOS, chemokine signaling was enriched in CD8_C1_GZMB cells, and antigen processing was prominent in CD8_C2_XCL1 cells. These results suggest OXPHOS affects tumor survival and immune function, with metabolic changes, like increased ROS production, potentially suppressing T cell activation and promoting immune evasion^{33,34}. Additionally, differential expression of OXPHOS and antigen presentation in stromal cells (Fibroblast_COL3A1 and Pericyte_ACTA2) indicates that metabolic shifts in the TME influence immune responses. In summary, OXPHOS in LSCC supports tumor growth and modulates immune responses, offering a potential therapeutic target.

In the context of laryngeal cancer, MDSCs play a critical role in modulating the immune landscape, which significantly impacts disease progression and response to therapy³⁵. MDSCs are a heterogeneous population of cells originating from the bone marrow and are known for their potent immunosuppressive activities. Their function in laryngeal cancer, as in many other malignancies, centers on their ability to inhibit T-cell mediated immune responses, which are crucial for anti-tumor immunity³⁶. However, limited research on the roles of Macrophage in the development and progression of LSCC has restricted further understanding. In this study, we identified characteristics of the TME in LSCC tumor tissues. Our scRNA-seq analysis results showed that the numbers of Macrophage-C1QC cells were increased in the LSCC tumor tissues than those in its adjacent tissues. The results is consistent with the reported that MDSCs show a pro-tumor effect³⁷.

The *PPIF* gene, encoding Cyclophilin D, is an integral part of the mitochondrial permeability transition pore and plays a significant role in regulating mitochondrial function and cell death. In the context of cancer, *PPIF* has been implicated in various mechanisms that contribute to tumorigenesis and tumor progression, including alterations in cellular metabolism, resistance to apoptosis, and the modulation of the tumor microenvironment³⁸. *PPIF* is known to influence cancer cell survival and proliferation through its effects on mitochondrial integrity and apoptosis. Overexpression of *PPIF* in cancer cells has been associated with increased resistance to apoptosis, a hallmark of cancer progression. This resistance is primarily mediated by *PPIF*'s ability to inhibit the mitochondrial permeability transition, thereby preventing cytochrome c release and subsequent activation of the caspase cascade essential for apoptotic cell death.

In the TME, particularly in the context of laryngeal cancer, *PPIF* may play a role in shaping the function and activity of MDSCs. MDSCs are known for their ability to suppress T-cell mediated immune responses, thereby promoting tumor immune evasion. The interaction between *PPIF* and MDSCs could potentially be through the regulation of mitochondrial functions, which are pivotal for the survival and immunosuppressive activity of these cells. MDSCs utilize various metabolic pathways to support their immunosuppressive functions, and *PPIF* could influence these pathways by regulating mitochondrial calcium uptake and protecting against mitochondrial dysfunction under the stressful conditions of the TME. Enhanced survival and functionality of MDSCs due to *PPIF* could lead to increased immunosuppression within the TME, thereby facilitating tumor growth and progression³⁹.

In this study, pseudo-time analysis provides valuable insights into the functional evolution of immune cells, particularly macrophages, within TME. Trajectory analysis of the Macrophage-C1-C1QC subgroup reveals how cell states evolve over time and their relevance to tumor pathophysiology. Specifically, *PPIF*_low macrophages exhibit a pro-inflammatory phenotype associated with anti-tumor activities such as phagocytosis and T-cell activation, whereas *PPIF*_high macrophages are linked to a suppressive environment that fosters

tumor progression. The pseudo-time trajectory effectively captures how these cells adapt to support processes like angiogenesis and invasion. This approach not only deepens our understanding of macrophage diversity but also highlights potential therapeutic targets and the optimal timing for intervention.

Given its role in both cancer cell survival and the modulation of the immune response, targeting *PPIF* could be a promising therapeutic strategy. Inhibitors of *PPIF*, such as cyclosporin A, have shown potential in preclinical models by inducing cancer cell apoptosis and reducing the suppressive functions of MDSCs, thus enhancing immune-mediated tumor suppression⁴⁰. Studies have also suggested that high expression of *PPIF* may be associated with poor clinical outcomes in LSCC patients, including decreased survival and increased risk of metastasis. In addition, blocking the *PPIF* protein using monoclonal antibodies has been shown to inhibit the proliferation of LSCC cells and promote apoptosis, suggesting that *PPIF* may be a potential therapeutic target for LSCC. The presence of *PPIF* expression within exosomes as revealed by our analysis suggests the potential involvement of these vesicles in intercellular communication and immune modulation. However, comprehensive investigations are warranted to fully elucidate the underlying mechanisms and functions associated with this phenomenon. The study of *PPIF* gene expression in exosomes may have implications for the diagnosis and treatment of immune-related diseases.

This macrophage subgroup division based on *PPIF* expression levels and its differential gene analysis not only provides a new perspective for understanding the complex role of macrophages in tumor biology, but also provides potential targets for the development of macrophage-mediated tumor treatment strategies. These findings will help promote the development of personalized tumor treatment, especially in regulating the activity of macrophages in the tumor microenvironment.

This study provides valuable insights into the role of *PPIF* and OXPHOS in LSCC, highlighting their impact on both cancer progression and immune evasion within TME. In addition to the key metabolic pathways identified, several other biomarkers and pathways could be targeted for immunotherapy in LSCC. For instance, immune checkpoint inhibitors targeting PD-1/PD-L1^{41,42}, which have shown promise in other cancers, could also enhance T-cell-mediated immune responses in LSCC. Additionally, targeting chemokine signaling pathways, particularly those associated with CD8 + T cells, could modulate immune cell trafficking to the tumor site, improving anti-tumor immunity. Furthermore, modulating antigen processing and presentation pathways, especially in stromal cells, could enhance immune cell recognition of tumor antigens. These approaches may complement existing treatments and improve the efficacy of immunotherapy in LSCC.

However, there are limitations to this study. The scRNA-seq analysis was based on a small sample size, which may not fully capture the heterogeneity of LSCC. Larger cohorts are needed for broader validation. While we identified key pathways like OXPHOS and *PPIF* expression, further experimental studies are necessary to confirm their roles in tumor progression and immune modulation. The molecular interactions between *PPIF* and immune cells, particularly MDSCs, remain unclear and warrant further investigation. Additionally, the therapeutic potential of *PPIF*-targeted interventions requires preclinical and clinical validation to assess their safety and efficacy. Further research into the mechanisms of *PPIF* in LSCC is essential, offering a dual target for therapeutic interventions that could improve outcomes in LSCC and potentially other malignancies.

Data availability

The accession number for the scRNA-seq data and exosome data described in this article is Gene Expression Omnibus Archive: PRJNA975301. To corroborate our scRNA-seq discoveries, one HNSC clinical dataset from the GEPIA2 data portal was employed in this investigation (available at <http://gepia2.cancer-pku.cn>).

Received: 12 October 2024; Accepted: 7 March 2025

Published online: 24 March 2025

References

1. Siegel, R. L., Miller, K. D., Fuchs, H. E. & Jemal, A. Cancer statistics, 2021. *CA Cancer J. Clin.* **71**, 7–33. <https://doi.org/10.3322/caac.21654> (2021).
2. Steuer, C. E., El-Deiry, M., Parks, J. R., Higgins, K. A. & Saba, N. F. An update on larynx cancer. *CA Cancer J. Clin.* **67**, 31–50. <https://doi.org/10.3322/caac.21386> (2017).
3. Wang, N. et al. PRMT5/Wnt4 axis promotes lymph-node metastasis and proliferation of laryngeal carcinoma. *Cell. Death Dis.* **11**. <https://doi.org/10.1038/s41419-020-03064-x> (2020).
4. Song, L. et al. Cellular heterogeneity landscape in laryngeal squamous cell carcinoma. **147**, 2879–2890 (2020).
5. Zheng, C. et al. Landscape of infiltrating T cells in liver cancer revealed by single-cell sequencing. *Cell* **169**, 1342–1356. <https://doi.org/10.1016/j.cell.2017.05.035> (2017).
6. D'Avola, D. et al. High-density single cell mRNA sequencing to characterize Circulating tumor cells in hepatocellular carcinoma. *Sci. Rep.* **8**. <https://doi.org/10.1038/s41598-018-30047-y> (2018).
7. Xu, Z., Zeng, S., Gong, Z., Yan, Y. J. M.C. Exosome-based immunotherapy: A promising approach for cancer treatment. **19**, 1–16. (2020).
8. Nasser, J. et al. Genome-wide enhancer maps link risk variants to disease genes. *Nature* **593**, 238–243. <https://doi.org/10.1038/s41586-021-03446-x> (2021).
9. Priber, J. et al. Cyclophilin D disruption attenuates lipopolysaccharide-induced inflammatory response in primary mouse macrophages. *Biochem. Cell Biol.* **93**, 241–250. <https://doi.org/10.1139/bcb-2014-0120> (2015).
10. Hao, Q. et al. Single-cell transcriptomes reveal heterogeneity of high-grade serous ovarian carcinoma. *Clin. Transl. Med.* **11**, e500. <https://doi.org/10.1002/ctm2.500> (2021).
11. Tay, R. E., Richardson, E. K. & Toh, H. C. Revisiting the role of CD4⁺ T cells in cancer immunotherapy-new insights into old paradigms. *Cancer Gene Ther.* **28**, 5–17. <https://doi.org/10.1038/s41417-020-0183-x> (2021).
12. Azizi, E. et al. Single-cell map of diverse immune phenotypes in the breast tumor microenvironment. **174**, 1293–1308 (2018).
13. Lauer, S. & Gresham, D. An evolving view of copy number variants. *Curr. Genet.* **65**, 1287–1295. <https://doi.org/10.1007/s00294-019-00980-0> (2019).

14. Liu, J. et al. SPINK5 is a prognostic biomarker associated with the progression and prognosis of laryngeal squamous cell carcinoma identified by weighted gene Co-Expression network analysis. *Evol. Bioinform. Online* **18**, <https://doi.org/10.1177/11769343221077118> (2022).
15. Li, C. et al. *Escherichia coli* O88 induces intestinal damage and inflammatory response through the oxidative phosphorylation and ribosome pathway in Pekin ducks. *Front. Cell. Infect. Microbiol.* **12**, 940847. <https://doi.org/10.3389/fcimb.2022.940847> (2022).
16. Zhang, L. et al. Lineage tracking reveals dynamic relationships of T cells in colorectal cancer. **564**, 268–272 (2018).
17. Li, H. et al. Dysfunctional CD8 T cells form a proliferative, dynamically regulated compartment within human melanoma. **176**, 775–789 (2019).
18. Guo, X. et al. Global characterization of T cells in non-small-cell lung cancer by single-cell sequencing. **24**, 978–985 (2018).
19. Kanehisa, M., Furumichi, M., Tanabe, M., Sato, Y. & Morishima, K. KEGG: New perspectives on genomes, pathways, diseases and drugs. *Nucleic Acids Res.* **45**, D353–D361. <https://doi.org/10.1093/nar/gkw1092> (2017).
20. Vento-Tormo, R. et al. Single-cell reconstruction of the early maternal–fetal interface in humans. **563**, 347–353. (2018).
21. Tang, Z., Kang, B., Li, C., Chen, T. & Zhang, Z. GEPIA2: An enhanced web server for large-scale expression profiling and interactive analysis. *Nucleic Acids Res.* **47**, W556–W560. <https://doi.org/10.1093/nar/gkz430> (2019).
22. Zhang, W. et al. N.A.R. COVID19db: A comprehensive database platform to discover potential drugs and targets of COVID-19 at whole transcriptomic scale. **50**, D747–D757 (2022).
23. Jin, S. et al. Inference and analysis of cell–cell communication using cellchat. *Nat. Commun.* **12**, 1088. <https://doi.org/10.1038/s41467-021-21246-9> (2021).
24. Hornburg, M. et al. Single-cell dissection of cellular components and interactions shaping the tumor immune phenotypes in ovarian cancer. *Cancer Cell.* **39**, 928–944e926. <https://doi.org/10.1016/j.ccell.2021.04.004> (2021).
25. Korsunsky, I. et al. Fast, sensitive and accurate integration of single-cell data with harmony. *Nat. Methods* **16**, 1289–1296. <https://doi.org/10.1038/s41592-019-0619-0> (2019).
26. Zhang, W. et al. COVID19db: A comprehensive database platform to discover potential drugs and targets of COVID-19 at whole transcriptomic scale. *Nucleic Acids Res.* **50**, D747–D757. <https://doi.org/10.1093/nar/gkab850> (2022).
27. Yu, G., Wang, L. G., Han, Y. & He, Q. Y. ClusterProfiler: An R package for comparing biological themes among gene clusters. *OMICS* **16**, 284–287. <https://doi.org/10.1089/omi.2011.0118> (2012).
28. Brodin, P. Immune determinants of COVID-19 disease presentation and severity. *Nat. Med.* **27**, 28–33. <https://doi.org/10.1038/s41591-020-01202-8> (2021).
29. Boschert, V., Teusch, J., Muller-Richter, U. D. A., Brands, R. C. & Hartmann, S. PKM2 modulation in head and neck squamous cell carcinoma. *Int. J. Mol. Sci.* **23**. <https://doi.org/10.3390/ijms23020775> (2022).
30. Frederick, M., Skinner, H. D., Kazi, S. A., Sikora, A. G. & Sandulache, V. C. High expression of oxidative phosphorylation genes predicts improved survival in squamous cell carcinomas of the head and neck and lung. *Sci. Rep.* **10**, 6380. <https://doi.org/10.1038/s41598-020-63448-z> (2020).
31. Uslu, C., Kapan, E. & Lyakhovich, A. Cancer resistance and metastasis are maintained through oxidative phosphorylation. *Cancer Lett.* **587**, 216705. <https://doi.org/10.1016/j.canlet.2024.216705> (2024).
32. Vander Heiden, M. G., Cantley, L. C. & Thompson, C. B. Understanding the Warburg effect: The metabolic requirements of cell proliferation. *Science* **324**, 1029–1033. <https://doi.org/10.1126/science.1160809> (2009).
33. Arner, E. N. & Rathmell, J. C. Metabolic programming and immune suppression in the tumor microenvironment. *Cancer Cell.* **41**, 421–433. <https://doi.org/10.1016/j.ccell.2023.01.009> (2023).
34. Schärping, N. E. et al. Mitochondrial stress induced by continuous stimulation under hypoxia rapidly drives T cell exhaustion. *Nat. Immunol.* **22**, 205–215. <https://doi.org/10.1038/s41590-020-00834-9> (2021).
35. Condamine, T., Mastio, J. & Gabrilovich, D. I. Transcriptional regulation of myeloid-derived suppressor cells. *J. Leukoc. Biol.* **98**, 913–922. <https://doi.org/10.1189/jlb.4RI0515-204R> (2015).
36. Kumar, V., Patel, S., Tcyganov, E. & Gabrilovich, D. I. The nature of Myeloid-Derived suppressor cells in the tumor microenvironment. *Trends Immunol.* **37**, 208–220. <https://doi.org/10.1016/j.it.2016.01.004> (2016).
37. Tirosh, I. et al. Dissecting the multicellular ecosystem of metastatic melanoma by single-cell RNA-seq. *Science* **352**, 189–196. <https://doi.org/10.1126/science.aad0501> (2016).
38. Guan, B. et al. Dissecting prostate cancer: Single-Cell insight into macrophage diversity, molecular prognosticators, and the role of Peptidylprolyl isomerase F. *Int. Immunopharmacol.* **138**, 112599. <https://doi.org/10.1016/j.intimp.2024.112599> (2024).
39. Biswas, S. K. & Lopez-Collazo, E. Endotoxin tolerance: New mechanisms, molecules and clinical significance. *Trends Immunol.* **30**, 475–487. <https://doi.org/10.1016/j.it.2009.07.009> (2009).
40. Grover, A., Sanseviero, E., Timosenko, E. & Gabrilovich, D. I. Myeloid-Derived suppressor cells: A propitious road to clinic. *Cancer Discov.* **11**, 2693–2706. <https://doi.org/10.1158/2159-8290.CD-21-0764> (2021).
41. Idel, C. et al. Correlation of Intra-tumoral and peripheral PD-1/CD-274 immunity in head and neck Cancer. *Anticancer Res.* **43**, 5349–5358. <https://doi.org/10.21873/anticancer.16738> (2023).
42. Tudor, F., Marijic, B., Babarovic, E. & Hadzisejdic, I. Significance of PD-L1 and tumor microenvironment in laryngeal squamous cell Cancer. *Cancers* **16**. <https://doi.org/10.3390/cancers16152645> (2024).

Acknowledgements

The authors thank each member of Zhang Lab for their suggestions.

Author contributions

Conceptualization, D.Z., Jianchao W. and X.W.; methodology, D.Z., Jianchao W., X.W., C.L., and T.W.; validation, L.T., Jiangyan W., W.Z. and Y.L.; formal analysis, Jianchao W., X.W., and C.L.; investigation, Y.L. and L.Y.; resources, Y.W. and F.Z.; data curation, L.T. and Jiangyan W.; writing—original draft preparation, Jianchao W., C.L., and T.W.; writing—review and editing, D.Z. and X.W.; visualization, L.T. and Jiangyan W.; supervision, D.Z. and X.W.; project administration, D.Z. and X.W.; funding acquisition, D.Z. (Shenzhen High-level Hospital Construction Fund) and X.W. (National Natural Science Foundation of China (No.82260475) and Major Scientific and Technological Innovation Project in the Health Industry of Gansu Province (No.GSWSD2024-02)). All authors reviewed this manuscript.

Declarations

Competing interests

The authors declare no competing interests.

Additional information

Supplementary Information The online version contains supplementary material available at <https://doi.org/10.1038/s41598-025-93584-3>.

Correspondence and requests for materials should be addressed to X.W. or D.Z.

Reprints and permissions information is available at www.nature.com/reprints.

Publisher's note Springer Nature remains neutral with regard to jurisdictional claims in published maps and institutional affiliations.

Open Access This article is licensed under a Creative Commons Attribution-NonCommercial-NoDerivatives 4.0 International License, which permits any non-commercial use, sharing, distribution and reproduction in any medium or format, as long as you give appropriate credit to the original author(s) and the source, provide a link to the Creative Commons licence, and indicate if you modified the licensed material. You do not have permission under this licence to share adapted material derived from this article or parts of it. The images or other third party material in this article are included in the article's Creative Commons licence, unless indicated otherwise in a credit line to the material. If material is not included in the article's Creative Commons licence and your intended use is not permitted by statutory regulation or exceeds the permitted use, you will need to obtain permission directly from the copyright holder. To view a copy of this licence, visit <http://creativecommons.org/licenses/by-nc-nd/4.0/>.

© The Author(s) 2025